Proceedings of ASME Turbo Expo 2011
GT2011
June 6-10, 2011, Vancouver, British Columbia, Canada

GT2011-45566

PREDICTION OF SEPARATION-INDUCED TRANSITION ON HIGH LIFT LOW PRESSURE TURBINE BLADE

Abdelkader Benyahia
Ph.D. Student – ONERA – DAAP
8 Rue des Vertugadins,
92190 Meudon, France
abdelkader.benyahia@onera.fr

Lionel Castillon
Research Engineer – ONERA – DAAP
8 Rue des Vertugadins,
92190 Meudon, France
lionel.castillon@onera.fr

Robert Houdeville
Research Engineer – ONERA – DMAE
2 Av. Edouard Belin,
BP 4025, 31055 Toulouse Cedex 4, France
robert.houdeville@onera.fr

ABSTRACT

This paper deals with the development and validation of the Menter and Langtry correlation-based transition model in the RANS code *elsA*. Two types of experimental linear cascades of low pressure turbine (LPT) airfoils having different loading distributions have been considered for the validation: the T106C and T108 blades. Experimental data have been provided by the Von Karman Institute in the framework of the European program TATMo. Different Reynolds numbers varying from 80 000 to 250 000 and different freestream turbulence intensities have been investigated. The results obtained for the T106C blade are in good agreement with the experimental data: the bubble size and the kinetic energy losses are well predicted. Sensitivity to freestream turbulence is also well demonstrated for the considered Reynolds numbers. However the results for the T108 blade show the limitations of the current version. These limitations are explained and discussed in this paper. The second part of this paper deals with the numerical and physical aspects of periodical unsteady inlet conditions which are introduced in order to take into account the incoming wakes. The original Menter and Langtry transition model has required a modification for performing correct unsteady computations of wake induced transition which is discussed in this paper. The unsteady results obtained with *elsA* are in quite good agreement with the experimental data.

NOMENCLATURE

c	Blade chord
M	Mach number
S	Strain rate magnitude
Tu	Turbulence Intensity
U	Local velocity
Ω	Vorticity magnitude
γ	Intermittency
Re	Reynolds number
Re_v	Vorticity Reynolds Number
$Re_{\theta t}$	Transition onset momentum thickness Reynolds number (from correlation)
$\tilde{Re}_{\theta t}$	Local transition onset momentum thickness Reynolds number (from transport equation)
λ_θ	Thwaites pressure gradient parameter
ρ	Density
y	Distance to the nearest wall
y^+	Normalized distance to the nearest wall
k	Turbulent kinetic energy
ω	Specific turbulence dissipation rate
μ	Molecular viscosity
μ_t	Turbulent viscosity
δ	Boundary Layer thickness
θ	Momentum thickness
ξ	Kinetic energy loss coefficient

Subscripts

0	Total condition
1	Upstream condition
2	Downstream condition
ax	Axial
is	Isentropic
sep	Separation
eff	Effective

Copyright © 2011 by ASME

INTRODUCTION

Typical Low Pressure Turbine (LPT) of modern bypass turbofan engines are composed of several stages and contributes around 1/3 of the engine overall weight. In order to reduce the weight of the LPT, the trends have been toward decreasing the number of blades while maintaining the same amount of stage work. Reduction of blade number also permits a reduction of the manufacturing and maintenance costs. As a consequence the loading per blade has been increased leading to the well known concept of "high lift design" [1]. Because an increase of 1% of the LPT efficiency or a decrease of 8% of weight leads to a reduction of 1% of the specific fuel consumption (SFC) the concept of "high loaded blade" has been, for several years, a subject of main interest for LPT designers [1].

At altitude cruise conditions the LPT turbine works at relative low Reynolds numbers. Typically, Reynolds numbers encountered at cruise altitude are about 100 000 [2]. Such low Reynolds numbers result in a laminar boundary layer forming on the suction side of the blades. It is well known that a laminar boundary layer is unable to overcome an important adverse pressure gradient. Due to the high lift concept and the resulting intense adverse pressure gradient, the laminar boundary layer presents on the suction side may separate. Downstream the separation point boundary layer transition is triggered and, in the most favorable case, the boundary layer rapidly reattaches in a turbulent state. A short laminar separation bubble therefore exists on the blade. The phenomenon of transition triggered by separation bubble was described by Horton [3] and by Hatman and Wang [4-6] in a general scope. The role of laminar to turbulent transition in gas turbines engines was described more precisely by Mayle [7]. Horton and Howell have described the specificities of laminar to turbulent transition in LPT [2]. The size of the bubble depends on the relative Reynolds number, the freestream turbulence level intensity, the adverse pressure gradient and other physical parameters. For constant freestream conditions (turbulence intensity and adverse pressure gradient) when lowering the Reynolds number the bubble size increases. Firstly, the passage of a short bubble to a long bubble, also named bursting, is observed. Then, for extreme low Reynolds numbers massive separation takes place and the boundary layer does not reattach. This situation is the most unfavorable because the losses are directly linked to the bubble size: the losses will be higher according to the length of the bubble.

However, in real environment, flow field in a turbine stage is essentially unsteady due to the relative motions between rotors and stators [2]. Unsteady wakes shed coming from the upstream stage strongly affect the separation induced transition process: the periodical incoming wakes, which are zones of high turbulence level intensity, promote the transition process. The incoming wakes can cause beneficial effects by reducing a long separation bubble to a small bubble or, eventually, completely suppressing separation of the boundary layer [8-10]. After the passage of the wake, calming phenomenon is observed and the bubble re-forming is more or less rapid. This phenomenon is still not completely understood and source of numerous studies [11].

Transition prediction is a main challenge for LPT aerodynamics but the simulation of the phenomenon remains a major challenge in Computational Fluid Dynamics (CFD). Obviously Direct Numerical Simulation would be the best solution for describing accurately transitional flows but, due to the extensive computational effort required, its use on real geometries or problems of practical relevance is years away. Large Eddy Simulation [12-14] have been performed for transionnal LPT flows but it is still limited to two dimensional (2D) or quasi three dimensional experimental configurations. RANS and URANS methods remain the only presently applicable method in an industrial context when dealing with transitional flows such as LPT flows. Most modern RANS codes include transition prediction capability by the mean of transition criterion coupled with turbulence model. However the use of transition criterion in RANS codes is still problematic from a numerical point of view. The γ - $\tilde{Re}_{\theta t}$ model proposed by Menter and Langtry [15,16] overcomes these difficulties by predicting transition only by the use of local quantities. The model does not attempt to model the physics of transition but proposes a framework for implementing empirical correlations based transition criteria in a general purpose flow solver with structured or unstructured parallelized solver. Because the model is only based on local quantities it represents a promising way to include possible transitional effects to be automatically taken in account in complex three dimensional RANS simulations. The model is based on two transport equations: one for the intermittency γ and the other one for the transition onset Reynolds number based on the momentum thickness $\tilde{Re}_{\theta t}$. The model has been initially incompletely published by Menter and Langtry [15], two functions were missing for proprietary reasons. Several research groups have paid attention to the Menter transition model and have proposed their own correlations for the missing functions [17-27]. Finally Langtry and Menter published in 2009 the model accompanied by the closure functions [28].

The γ - $\tilde{Re}_{\theta t}$ model has been implemented in the RANS code *elsA* developed at ONERA [29]. A calibration of the missing functions has been performed at ONERA by Content et al [27]. In the first part of this paper a description of the Menter and Langtry transition model is given. The model is completed by the correlations of Content et al [18] which are also presented. When dealing with unsteady wake induced transition it has been noticed that the model might require a slight modification. This modification is discussed and reported in this paper. In the second part of this paper the validation of the model for two LPT test cases is presented: steady two and three dimensional results obtained for the T106C [9,30] and T108 [31] blades are presented completed by unsteady quasi three dimensional results obtained for the T106C test case.

MODEL DESCRIPTION

Copyright © 2011 by ASME

The transport equation for the intermittency is formulated as follows:

$$\frac{\partial(\rho\gamma)}{\partial t}+\frac{\partial\left(\rho U_j\gamma\right)}{\partial x_j}=P_\gamma-E_\gamma+\frac{\partial}{\partial x_j}\left[\left(\mu+\frac{\mu_t}{\sigma_f}\right)\frac{\partial\gamma}{\partial x_j}\right] \quad (1)$$

In Eq. 1, P_γ and E_γ are source terms which control the production and destruction of intermittency and defined as follows:

$$P_\gamma=F_{length}c_{a1}\rho S\left[\gamma F_{onset}\right]^{0.5}(1-\gamma) \quad (2)$$

$$E_\gamma=c_{a2}\rho\Omega F_{turb}(c_{e2}\gamma-1) \quad (3)$$

with S the strain rate and Ω the vorticity magnitude. The constants used to tune the Eq. [1-3] are defined as follows: c_{e1}=1.0; c_{a1} =2.0; c_{e2} =50.0; c_{a2} = 0.06 ; σ_f =1.0. The function F_{turb} presents in Eq. 3 is defined as:

$$F_{turb}=e^{-(R_T/4)^4} \quad (4)$$

$$R_T=\frac{\rho k}{\mu\omega} \quad (5)$$

Van Driest and Blummer [32] have highlighted that for Blasius laminar boundary layer:

$$Re_\theta=\frac{Re_{v,max}}{2.193} \quad (6)$$

where Re_v is the local vorticity Reynolds number defined as:

$$Re_v=\frac{\rho y^2}{\mu}\frac{\partial U}{\partial y}=\frac{\rho y^2}{\mu}S \quad (7)$$

By comparing locally Re_v and a critical local momentum thickness Reynolds number for the transition onset the intermittency production can be possibly turned on. The function F_{onset} which triggers the intermittency production is based on that assumption and defined as:

$$F_{onset1}=\frac{Re_v}{2.193\,Re_{\theta c}} \quad (8\text{-a})$$

$$F_{onset2}=min\left[max(F_{onset1},F_{onset1}{}^4),2.0\right] \quad (8\text{-b})$$

$$F_{onset3}=max\left[1-\left(\frac{R_T}{2.5}\right)^3,0.0\right] \quad (8\text{-c})$$

$$F_{onset}=max(F_{onset2}-F_{onset3},0.0) \quad (8\text{-d})$$

The aim of the second transport equation is to obtain locally this critical momentum thickness Reynolds number $Re_{\theta c}$ to compute F_{onset}. The transport equation for the transition momentum thickness Reynolds number reads:

$$\frac{\partial\left(\rho\tilde{Re}_{\theta t}\right)}{\partial t}+\frac{\partial\left(\rho U_j\tilde{Re}_{\theta t}\right)}{\partial x_j}=P_{\theta t}+\frac{\partial}{\partial x_j}\left[\sigma_{\theta t}\left(\mu+\mu_t\right)\frac{\partial\tilde{Re}_{\theta t}}{\partial x_j}\right] \quad (9)$$

$$P_{\theta t}=c_{\theta t}\frac{\rho}{t}\left(Re_{\theta t}-\tilde{Re}_{\theta t}\right)\left(1-F_{\theta t}\right) \quad (10)$$

$$t=\frac{500\mu}{\rho U^2} \quad (11)$$

t is a time scale present for dimensional reasons, $c_{\theta t}$ = 0.03 and $\sigma_{\theta t}$ = 10.0. $F_{\theta t}$ is a blending function which is equal to 1.0 in the boundary layer and null outside [15]. The definition of $F_{\theta t}$ is given and discussed latter in this paper. This function aims at distinguishing the boundary layer from the freestream. In Eq. 10 $Re_{\theta t}$ is obtained from transition onset correlation like the Abu-Ghannam and Shaw [33] or Mayle [7] correlations. Typically $Re_{\theta t}$ is a function of the local turbulence intensity level Tu and the Thwaites pressure gradient parameter λ_θ. The correlation of Langtry et al [16] has been employed in this study. Outside the boundary layer $\tilde{Re}_{\theta t}$ matches $Re_{\theta t}$ while in the boundary layer the values of $\tilde{Re}_{\theta t}$ at the edge of the latest are diffused. Since at the edge of the boundary layer $\tilde{Re}_{\theta t}$ is equal to the transition onset momentum thickness Reynolds number computed from a correlation $Re_{\theta t}$, in the boundary layer the latter is known locally through $\tilde{Re}_{\theta t}$. It is desirable for modeling aspect to slightly shift the critical transition onset Reynolds number used in F_{onset} computation to the value obtained directly from $\tilde{Re}_{\theta t}$ that is why $Re_{\theta c}$ is determined as a function of $\tilde{Re}_{\theta t}$ (Eq. 12) and employed in Eq.8-a.

$$Re_{\theta c}=f\left(\tilde{Re}_{\theta t}\right) \quad (12)$$

To close the transition model two functions had to be determined until Menter and Langtry published them: the function which links $Re_{\theta c}$ to $\tilde{Re}_{\theta t}$ (Eq. 12) and the function F_{length} employed in Eq. 2:

$$F_{length}=f\left(\tilde{Re}_{\theta t}\right) \quad (13)$$

The results presented in this paper are based on the ONERA in house correlations obtained by Content et al [27]:

$$Re_{\theta c}=min\left(1.0,1.623\cdot10^{-6}\tilde{Re}_{\theta t}^2-1.228\cdot10^{-3}\tilde{Re}_{\theta t}+0.849\right)\tilde{Re}_{\theta t} \quad (14)$$

$$F_{length}=exp\left(\begin{array}{r}-1.325\cdot10^{-8}\tilde{Re}_{\theta t}^3+7.42\cdot10^{-6}\tilde{Re}_{\theta t}^2\\+8.16\cdot10^{-3}\tilde{Re}_{\theta t}+2.5652\end{array}\right) \quad (15)$$

The transition model is coupled to the k-ω SST turbulence model [34] by modifying the production and destruction terms in the turbulent kinetic energy – k – equation:

$$P_k=\gamma_{eff}P_k \quad (16)$$

$$D_k=min\left(max\left(\gamma_{eff},0.1\right),1.0\right)D_k \quad (17)$$

$$\gamma_{eff}=max\left(\gamma,\gamma_{sep}\right) \quad (18)$$

where P_k and D_k on the right hand side of the Eq. [16-17] are the original production and destruction terms of the k-ω SST model [34]. The effective intermittency γ_{eff} (Eq. 18) which is employed in the turbulence model could be γ the intermittency obtained from the transport equation or γ_{sep} (Eq. 19) an intermittency function introduced by Menter and Langtry [28] in order to model separation induced transition. It has been

Copyright © 2011 by ASME

observed that, when dealing with separation induced transition issues with the *k-ω* SST model, production of turbulence downstream the transition onset may not permit a reattachment of the boundary layer [28]. Therefore the γ_{sep} function has been introduced by Menter and Langtry [28] in order to detect laminar boundary layer separation and to permit locally an over production of turbulent kinetic energy which will promote a reattachment of the boundary layer. This local over production of turbulent kinetic energy is achieved by allowing values of γ_{sep} to exceed 1.0

$$\gamma_{sep} = min\left\{ s_1 \cdot max\left[\left(\frac{Re_V}{3.235\,Re_{\theta c}} - 1.0 \right), 0.0 \right] F_{reattach}, 2. \right\} F_{\theta t} \quad (19)$$

$$F_{reattach} = exp\left(-\left(R_T / 20 \right)^4 \right) \quad (20)$$

Separation of the laminar boundary layer can be detected because when a laminar boundary layer separates the ratio $Re_v/2.193Re_{\theta c}$ goes to large values. The function $F_{reattach}$ makes the over production of turbulence energy being null when enough eddy viscosity is produced.

The constant s_1 (Eq. 19) controls the values of γ_{sep} and has a strong influence on the reattachment point because it will directly influence the over production of turbulent kinetic energy. As recently demonstrated by Corral and Gisbert [24] and other research groups [25,26][35,36] who employed the Menter transition model for modeling separation induced transition a constant value for s_1 will not permit a satisfying modeling of separation induced transition in a general framework. The reattachment point of the boundary layer is different from a test case to another one depending on several physical parameters such as the freestream turbulence intensity or the adverse pressure gradient. While adopting a constant value for s_1 it seems to be impossible to model the complex phenomenon of separation induced transition for a large range of different freestream conditions. Corral and Gisbert [24] tried to introduce a dependency of s_1 to $\tilde{Re}_{\theta t}$ in order to obtain the closest possible agreement between CFD results and experimental data for the T106C and T108 test case. However the Fs_1 function published by Corral and Gisbert [24] is in fact constant and equal to 3.0 so no real dependency has been introduced. They succeed in matching experimental data with CFD predictions for the T108 test case but unfortunately the numerical results remained unsatisfying for the T106C test case. In this study we used, as published by Menter and Langtry [28], a constant value for $s_1=2.0$. The blending function $F_{\theta t}$ is present in Eq. 19 in order to assign the possible over production of turbulence kinetic energy only inside the boundary layer where per definition $F_{\theta t}$=1.0.

Modification of $F_{\theta t}$

It has been noticed when dealing with unsteady wake induced transition computations that $F_{\theta t}$ may be equal to 1.0 outside the boundary layer. This shortcoming derivates from the definition of $F_{\theta t}$:

$$F_{\theta t} = min\left(max\left[F_{wake}\, e^{-\left(\frac{y}{\delta}\right)^4}, 1.0 - \left(\frac{\gamma - 1/c_{e2}}{1.0 - 1/c_{e2}} \right) \right], 1.0 \right) \quad (21)$$

$$F_{wake} = e^{-\left(\frac{Re_\omega}{10^5}\right)^2}; \quad Re_\omega = \frac{\rho y^2 \omega}{\mu} \quad (22)$$

$$\delta = \frac{375 \tilde{Re}_{\theta t} \mu y \Omega}{\rho U^2} \quad (23)$$

As it is pointed out by Eq. 23 the ratio y/δ (Eq. 21) is only a function of the local velocity and the vorticity magnitude Ω. If the vorticity becomes sufficiently large, which may happen in the blade channel when an upstream incoming wake is passing [10,13], $F_{\theta t}$ can switch to 1.0 outside the boundary layer and strongly affect the $\tilde{Re}_{\theta t}$ equation (Eq. 9). Activation of over production of turbulent kinetic energy (Eq. 19) may also happen outside the boundary layer.

This discrepancy has been corrected by defining δ as follows:

$$\delta = \frac{75 \tilde{Re}_{\theta t} \mu \Omega t}{\rho U} \quad (24)$$

with t previously defined in Eq. 11. Therefore in Eq. 21 a dependency on the wall distance has been introduced for the ratio y/δ and for the blending function $F_{\theta t}$.

NUMERICAL METHOD

The results discussed in the following parts of this paper have been obtained with the ONERA in house code Navier-Stokes *elsA* [29]. This code solves the unsteady 3D RANS equations with a finite volume method based on a multi-domain approach on structured and chimera grids. The convective fluxes are discretized with the upwind method of Roe and diffusive fluxes are discretized with a second-order accurate central-differencing scheme. A Backward-Euler time integration scheme has been employed for both steady and unsteady computations. For the steady computations local time step with a scalar LU-SSOR implicitation method has been also employed. Concerning the transition variables, as proposed by Menter and Langtry [28], γ is set to 1.0 at the inlet of the computational domain and $\tilde{Re}_{\theta t}$ is set according to Langtry's correlation [28] with λ_θ=0.0. At wall boundaries zero flux condition is applied for both γ and $\tilde{Re}_{\theta t}$.

STEADY FLOW RESULTS

T106C Cascade

The T106C blade is a LPT "ultra high lift" blade profile [9,30]. This blade section has been widely studied in both experimental and numerical investigations. The

Copyright © 2011 by ASME

experimental data used here have been provided by Arts et al [30] who experimentally investigated the blade performance in the framework of the European project TATMo. The characteristics of the T106C cascade are summarized in Tab. 1

Chord c (mm)	93.01
Pitch to chord ratio (g/c)	0.95
Inlet flow angle (deg)	32.7
Outlet flow angle (deg)	60.58
M_{2is}	0.65

Tab. 1 T106C Main characteristics

Figure 1 shows the blade geometry and the 2D computational grid which consists in a classical O4H grid. This grid has been obtained by De Saint Victor [38] following a study concerning the error estimate due to the grid. The total number of grid nodes is about 36 600, y^+ maximum values are below 1 along the blade. The number of grid points has been on purpose limited for maintaining reasonable CPU costs and short resulting calculation time compatible with an use in an industrial context. Two inlet turbulence intensity levels *Tu* have been considered: 0.8% which corresponds to the measurements performed at the VKI [30] with the natural turbulence intensity level of the facility and 1.8% which corresponds to a level reached downstream a turbulence grid introduced in the facility upstream the blade leading edge. Reynolds numbers Re_{2is} based upon the isentropic exit Mach number M_{2is} and the blade chord *c* range between 80 000 and 250 000. At the inlet of the computational domain a turbulent to laminar viscosity ratio μ_t/μ = 0.1 has been imposed for the test case with a turbulence intensity level *Tu*=0.8% and μ_t/μ = 10.0 has been imposed for the test case with a turbulence intensity level *Tu*=1.8%. This ratio can have a strong influence on the CFD results as mentioned by Spalart and Rumsey [39]. For the highest turbulence intensity level test case, measurements of turbulence decay upstream the blade leading edge provided by Arts et al [30] allow to set a credible value of μ_t/μ in computations. For the lowest inlet turbulence level a low value of 0.01 [28] has been imposed.

Reynolds number effect

Figure 2 shows the midspan isentropic Mach number distributions along the blade for the considered Reynolds numbers. For all considered Reynolds numbers boundary layer separation occurs on the suction side in the adverse pressure gradient region. Separation is well visible on the isentropic Mach number plots: a small to long plateau appears in the decelerating region. The experimental data and the CFD results are in very good agreement. The isentropic Mach number peak is well captured as well as the separation point except for the

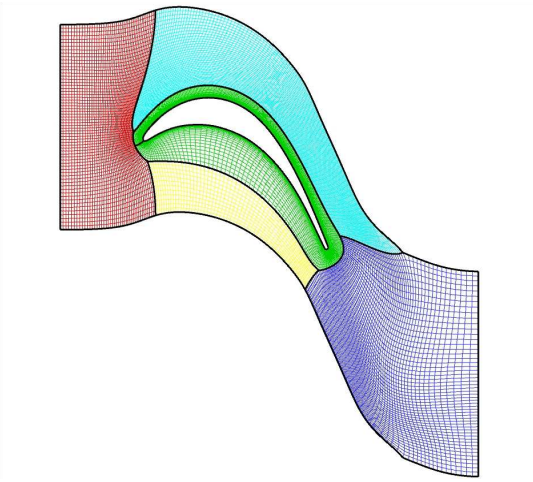

Fig. 1: 2D Computational Grid for the T106C cascade

lowest Reynolds number Re_{2is}=80 000. The reattachment point is also well captured. In the separated flow region the isentropic Mach number distributions obtained numerically match very well the ones obtained experimentally. A decrease of the Reynolds number leads to an increase of the pressure plateau size which corresponds to a growth of the bubble. The results obtained with the γ - $\tilde{Re}_{\theta t}$ reproduce quite well this tendency. According to Arts et al [30] bubble bursting occurs for Re_{2is}=140 000 while for Re_{2is} < 120 000 an open bubble takes place on the suction side. As it is visible in Fig. 3 the bubble topology is well predicted by CFD computations.

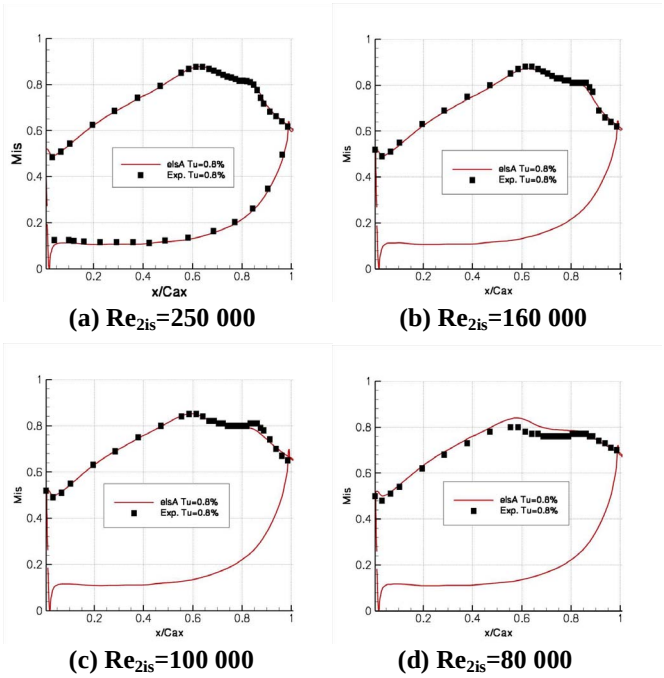

(a) Re_{2is}=250 000 **(b) Re_{2is}=160 000**

(c) Re_{2is}=100 000 **(d) Re_{2is}=80 000**

Fig. 2: Comparison between experimental and numerical values of M_{is} for the T106C cascade – *Tu*=0.8%

Copyright © 2011 by ASME

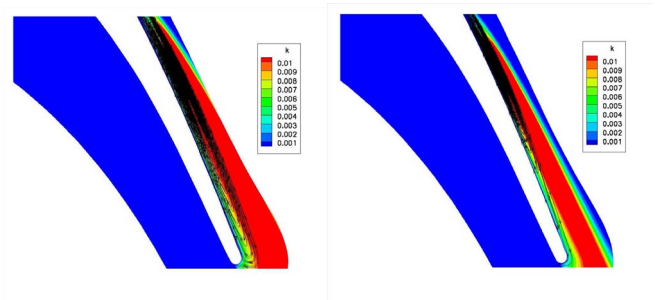

(a) Re_{2is}=100 000 **(b) Re_{2is}=120 000**

Fig. 3: Contours of non-dimensional turbulent kinetic energy for the T106C cascade – *Tu*=0.8% - Bubble topology

Figure 4 compares measured and calculated distributions of total pressure defect $(P_{01}-P_{02})/P_{01}$ as a function of the position along the blade pitch half a chord downstream the blade trailing edge. The peak value is under estimated in CFD but this discrepancy tends to be less important when the Reynolds number is lowered. The wake width is quite well estimated.

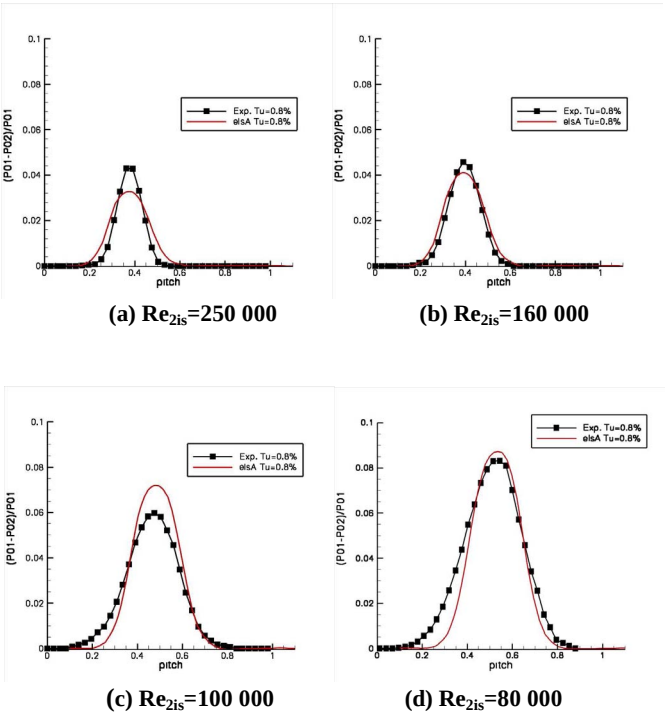

(a) Re_{2is}=250 000 **(b) Re_{2is}=160 000**

(c) Re_{2is}=100 000 **(d) Re_{2is}=80 000**

Fig. 4: Comparison between experimental and numerical values of the total pressure defects at *x/Cax*=1.5 for the T106C cascade – *Tu*=0.8%

Figures 6 and 7 compare experimental and numerical mass-averaged values of kinetic energy losses and the outlet flow angle at *x/Cax*=1.5. The kinetic energy loss coefficient is defined as:

$$\xi = 1 - \frac{1 - \left(\frac{\bar{P}_2}{\bar{P}_{02}}\right)^{\frac{\alpha-1}{\alpha}}}{1 - \left(\frac{\bar{P}_2}{\bar{P}_{01}}\right)^{\frac{\alpha-1}{\alpha}}}$$

with α=1.4

A very good agreement is obtained between the numerical and the experimental results. The differences between the numerical and the experimental results are less than 10% except for the lowest Reynolds number Re_{2is}=80 000 for which the discrepancies are more pronounced. The abrupt increase of losses for Re_{2is} < 140 000 due to the bubble growth is well predicted. The outlet flow angle is over predicted but the experimental tendency is well captured: when the Reynolds number is lowered the bubble size increases which will reduce the deviation of the flow. The differences between the numerical and the experimental results are about 1 degree except for the lowest Reynolds number Re_{2is}=80 000 for which the difference is about 2 degrees.

Turbulence intensity effect

Increasing the turbulence intensity level *Tu* has an evident effect on the isentropic Mach number distribution [30]: the transition process is promoted and the flow reattaches before the trailing edge. Bubble bursting is shifted to a lower critical Reynolds number and massive separation of the boundary layer is prevented. This beneficial effect is well visible on the experimentally measured kinetic energy losses which are significantly reduced for the lowest Reynolds numbers. For the range of studied Reynolds numbers the simulations at *Tu*=1.8% with the Menter transition model under predict the bubble size as illustrated in Fig. 5 which presents the isentropic Mach number distributions along the blade for a median and a low Reynolds number. The flow reattaches more rapidly in the computation than it is suggested by the experimental data.

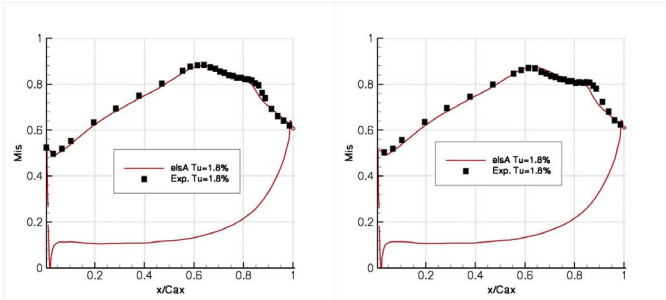

(a) Re_{2is}=160 000 **(b) Re_{2is}=100 000**

Fig. 5: Comparison between experimental and numerical values of M_{is} for the T106C cascade – *Tu*=1.8%

Copyright © 2011 by ASME

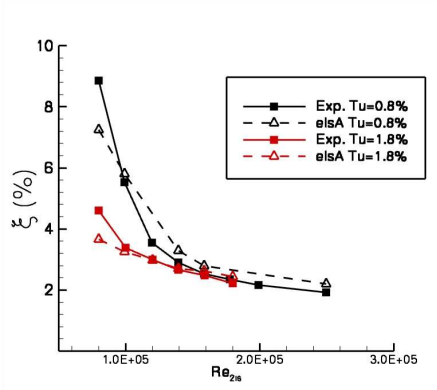

Fig. 6: Mass-weighted kinetic energy losses as a function of Re_{2is} for the T106C cascade

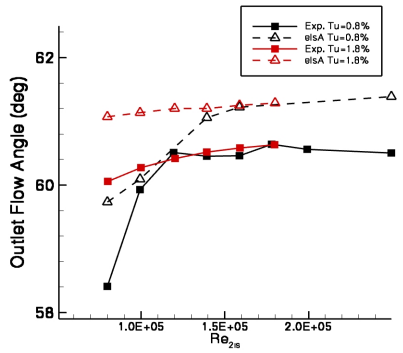

Fig. 7: Mass-weighted outlet flow angle as a function of Re_{2is} for the T106C cascade

When looking at the kinetic energy losses in Fig. 6 the beneficial effect of a turbulence intensity increase is well captured by calculation and the computational results are in good agreement with the measured values except for the lowest Reynolds number Re_{2is}=80 000. In fact the production of turbulence kinetic energy via γ_{sep} is too important which causes an early reattachment of the flow. However this has a priori here no consequence on the losses prediction. Arts et al [30] investigated three different inlet turbulence intensity levels: *Tu*=0.8%, *Tu*=1.8% and *Tu*=3.2%. The numerical and experimental results for *Tu*=3.2% are not presented in this paper. Arts et al [30] experimentally noticed that the kinetic energy losses are quite similar for *Tu*=1.8% and *Tu*=3.2% which may explain why, even if the bubble size for *Tu*=1.8% is under predicted in the computations with respect to the experimental data, the losses remain well predicted.

T108 Cascade

The T108 cascade is a high lift configuration also tested at the VKI in the framework of the European research program TATMo [31]. The blade loading of the T108 is different from the blade loading of the T106C: the blade is front loaded which as a consequence leads to a gradual diffusion downstream the velocity peak and thus to a lower adverse pressure gradient.

The blade characteristics are given in Tab. 2 below.

Chord c (mm)	93.01
Pitch to chord ratio (g/c)	1.05
Inlet flow angle (deg)	32.7
Outlet flow angle (deg)	60.5
M_{2is}	0.6

Tab. 2 T108 Main characteristics

The flow conditions are similar to those employed in the T106C cascade study: Reynolds numbers Re_{2is} ranging from 200 000 to 80 000 have been considered for an unique turbulence intensity level *Tu*=0.08%. Since the Menter transition model is dedicated to an intensive use in engineering in an industrial context, three dimensional (3D) computations have been performed for the T106C and T108 test cases. We have been able to verify, but not reported here, that isentropic Mach number distributions and kinetic losses remain unchanged at mid-span between the 2D and 3D simulations. The following results for the T108 blade are based on three dimensional computations. A blade to blade view at mid-span of the T108 geometry and the computational grid is visible in Fig. 8. The 3D mesh grid has about 1 876 00 nodes.

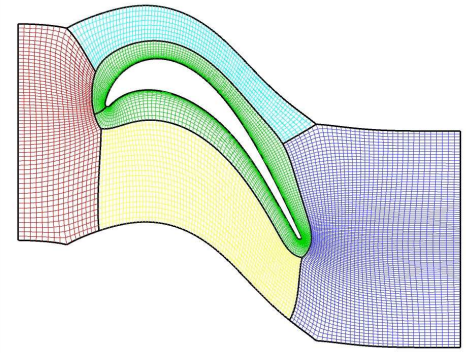

Figure 8- Blade to blade view at mid span of the T108 geometry and computational grid

Figure 9 compares calculated and measured isentropic Mach number distributions for various Reynolds numbers. For the high Reynolds number Re_{2is}=200 000 the peak velocity is well computed as well as the isentropic Mach number until boundary layer separation. The experimental results suggest the presence of a very small bubble between *x/Cax*=0.75 and *x/Cax*=0.85 even if no real plateau is visible on the isentropic Mach number distribution (Fig. 9-a2). The numerical results show a noticeable small plateau located at *x/Cax*=0.85 and a reattachment point at *x/Cax*=0.9. In fact it has been noticed that in computations

Copyright © 2011 by ASME

separation of the boundary layer occurs at *x/Cax*=0.75 but a small separated flow region remains confined in the vicinity of the wall. Therefore transition onset and reattachment are late predicted by the model. As a consequence the predicted bubble is thicker and longer which explains the discrepancies in terms of isentropic Mach number. Finally, the predicted mass averages losses for Re_{2is}=200 000 are more important compared to the measured losses (Fig. 10). When the Reynolds number is gradually lowered the bubble becomes more apparent on the experimental isentropic Mach number distributions which display a small plateau. Therefore the experimental and measured Mach number distributions are in better agreement for the lowest Reynolds numbers than for the highest ones except in the separated flow region. The numerical distributions indicate a pronounced bubble size while in the experimental data the bubble remains as short type and no bursting is observed. For the lowest Reynolds number Re_{2is}=80 000 the boundary separation is important in CFD computations.

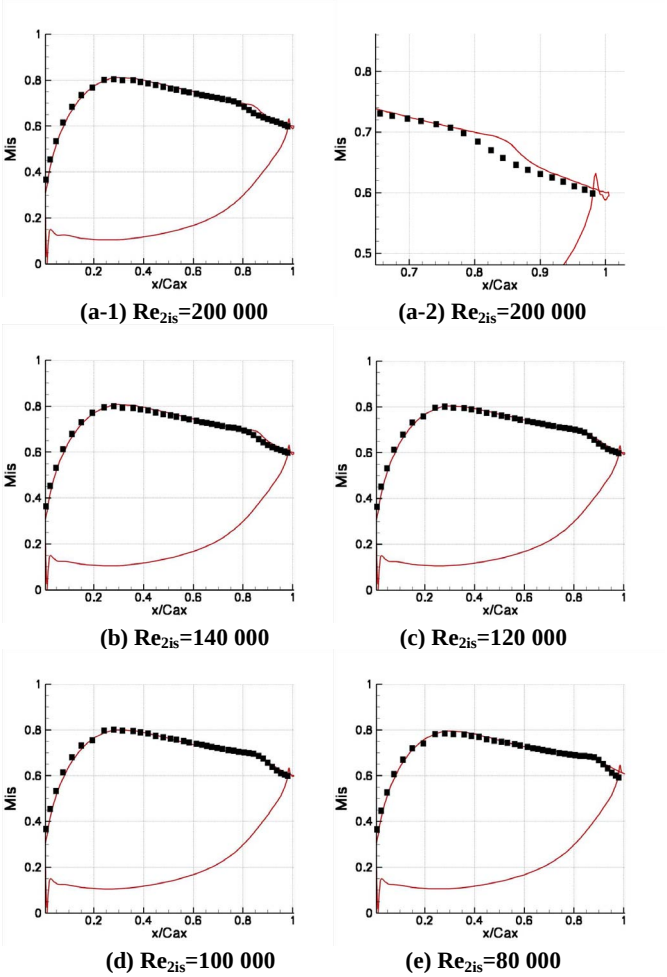

(a-1) Re_{2is}=200 000 **(a-2) Re_{2is}=200 000**

(b) Re_{2is}=140 000 **(c) Re_{2is}=120 000**

(d) Re_{2is}=100 000 **(e) Re_{2is}=80 000**

Fig. 9: Comparison between experimental and numerical values of M_{is} for the T108 cascade – *Tu*=0.8%

These discrepancies in terms of bubble topology strongly impact the prediction of downstream mass averaged kinetic losses: the losses are strongly over-estimated in CFD compared to measurements for the considered Reynolds numbers (Fig. 10). The differences between the numerical and the experimental results are about 10% for the higher Reynolds number Re_{2is}=200 000 but become more pronounced when the Reynolds number is lowered and reach 150%. The experimental tendency is not captured in CFD: when lowering the Reynolds number the measured losses remain quasi constant whereas the numerically evaluated losses strongly increase. These discrepancies are also noticeable in Fig. 11 which compares measured and calculated outlet flow angle as a function of the Reynolds number: the differences are about 1 degree and become more pronounced at relative low Reynolds numbers.

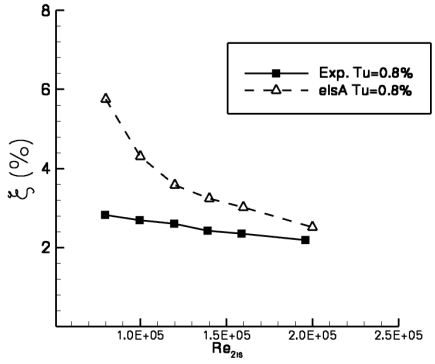

Fig. 10: Mass-weighted kinetic energy losses as a function of Re_{2is} for the T108 cascade

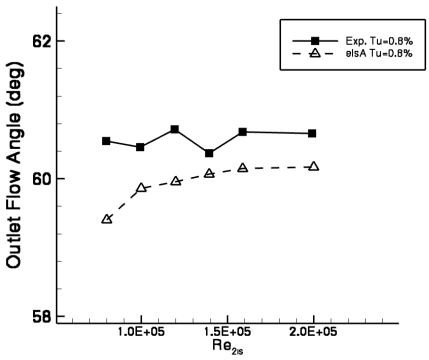

Fig. 11: Mass-weighted outlet flow angle as a function of Re_{2is} for the T108 cascade

Comparison of the results - Model Discussion

The results obtained with the Menter transition model for these two different blades, the ultra high lift T106C and the front loaded high lift T108, show two opposite tendencies. For the T106C case at *Tu*=1.8% the predicted bubble is too small while it is too large for the T108 test case at *Tu*=0.8%. These considerations suggest, in the bubble zone, an increase of the

Copyright © 2011 by ASME

values for γ_{sep} for the T108 test case and a decrease of the values for the T106C test case compared to those obtained with the current definition of γ_{sep}. The definition of γ_{sep} (Eq. 19) provided by Menter and Langtry [28] is not able to distinguish these two different bubble dynamics because it is only based on $Re_{\theta c}$ and constant definitions for s_1 and $F_{reattach}$ (Eq. 19). For achieving a better modeling of separation induced transition s_1 and/or $F_{reattach}$ have to be tuned and re-defined as functions of physical parameters. Another solution could consist in defining a new correlation for $Re_{\theta t}$ compared to the one proposed by Langtry [28] taking in account bypass and separation induced transition modeling which would lead to $Re_{\theta c}$ values well suited for both transition phenomenon modeling. Same conclusions have been formulated by other research groups which studied separation induced transition with the use of the Menter transition model [24-26] [35-37]. This is the next step of the current work performed at ONERA with the γ - $\tilde{R}e_{\theta t}$ model.

UNSTEADY FLOW RESULTS

In order to simulate the effect of incoming wakes on the T106C blade performance unsteady computations have been performed. The question of modeling the upstream experimental circular moving bars as part of the computational process of prescribing inlet-flow conditions has been treated by Lardeau and Leschziner [40]. They demonstrated the serious problems associated with vortex shedding treatment in the RANS approach and the implied numeral issues. They suggest, if experimental data describing the wake are available, to prescribe these latest as inlet-flow conditions. Prescribing the incoming wakes as part of the flow-inlet conditions upstream the blade passage is a simple way to simulate the influence of the upstream wakes shed. This strategy has been adopted in the present study and periodic profiles along one pitch of velocity, turbulent kinetic energy and total pressure have been prescribed at the inlet plan of the computational domain. Experimental data provided by the VKI during the European research program UTAT have been used to characterise the wake. The velocity deficit imposed is visible in Fig. 12 which displays the inlet velocity in the computational domain as a function of the pitch position. Computations have been performed for a Reynolds number Re_{2is}=100 000. Outside the wake the turbulence intensity level has been maintained to Tu=0.8%. The bar pitch matches with the cascade pitch leading to a reduce blade passage frequency f_r=0.68. All the computations have been carried out as quasi three dimensional calculations since we are only interested in the influence of the incoming wakes at mid-span. The same mesh as for the steady computations (Fig. 1) has been used. Lardeau and Leschziner [40] have recommended to use at least 800 time steps per wake period to reach an accurate description of the wake kinematics and the interactions between the wake and the boundary layer. In this study 1600 time steps per period have been imposed.

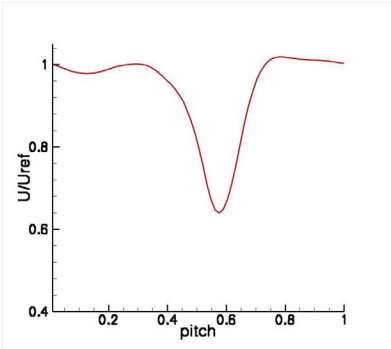

Figure 12: Prescribed inlet velocity profile for the unsteady computation on the T106C blade

Figure 13 visualizes the convection of the wake through the blade channel at four equally spaced time steps during one wake passage period. The distortion of the wake [41][13,14] is well captured and, as visible in Fig. 14, $\tilde{R}e_{\theta t}$ values are also well convected in the blade passage. Since the wake is a zone of high turbulence level intensity relative low values for $\tilde{R}e_{\theta t}$ are encountered in this zone.

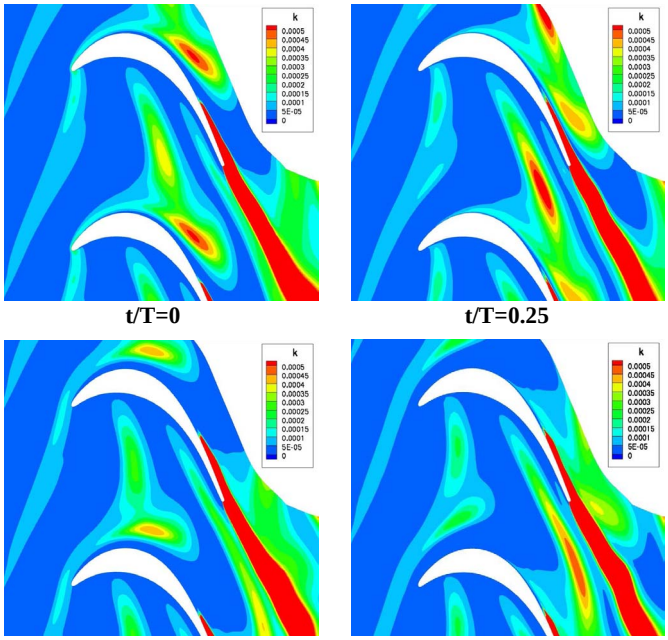

Figure 13: Non-dimensionalised turbulent kinetic energy contours in the T106C cascade through the wake passing

As mentioned in the first part of this paper the computations have been performed with a function $F_{\theta t}$ (Eq. 21) which was modified compared to the function of Menter and Langtry [16]. When using the original function $F_{\theta t}$, $\tilde{R}e_{\theta t}$ values in the blade channel became completely wrong and did not permit a good representation of the wake kinematics as it is visible in Fig. 14 which shows the contours of $\tilde{R}e_{\theta t}$ at $t/T=0.25$ obtained with the

Copyright © 2011 by ASME

original definition for $F_{\theta t}$. When looking at turbulent kinetic energy contours at *t/T=0.25* (Fig. 13), one may notice that the wake is not well modeled in terms of $\tilde{Re}_{\theta t}$ values (Fig. 14). On the other hand, the use of the modified $F_{\theta t}$ function leads to a well representation of the wake kinematics in terms of $\tilde{Re}_{\theta t}$ values as it is visible in Fig. 15.

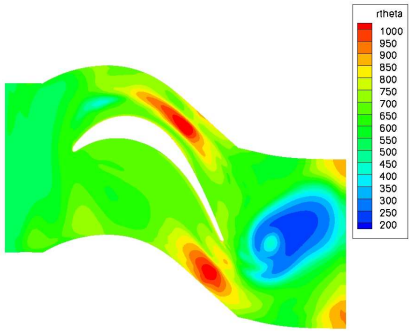

Figure 14: $\tilde{Re}_{\theta t}$ contours in the T106C cascade at t/T=0.25 obtained with the original definition of $F_{\theta t}$

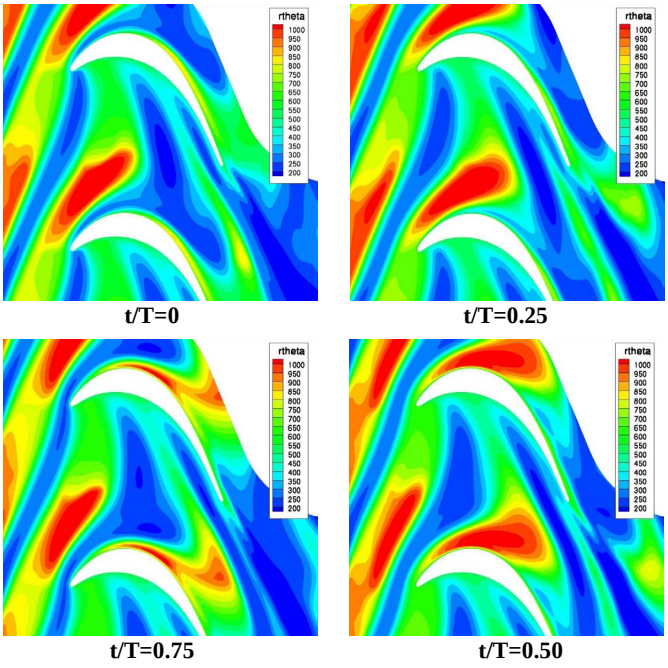

Figure 15: $\tilde{Re}_{\theta t}$ contours in the T106C cascade through the wake passing obtained with the modified function $F_{\theta t}$

Figure 16 presents space-time plot of the skin-friction coefficient on the blade suction side for Re_{2is}=100 000. The black lines materialise the separation and reattachment points.

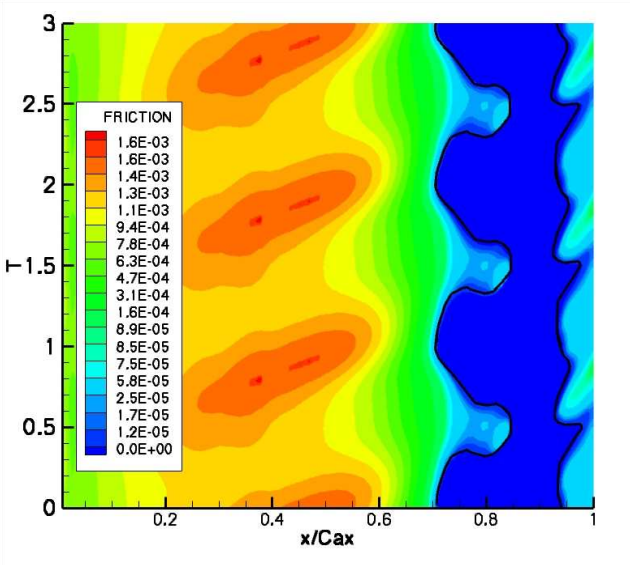

Figure 16: Space-Time plot of skin friction along the T106C cascade suction side at Re_{2is}=100 000

The periodic wakes interact with the boundary layer in the decelerating zone where for the steady case an open bubble is observed (Fig. 2-c). Compared to steady state results the periodic wake passage provokes a reattachment of the boundary layer before the trailing edge. The presence of an open bubble is not observed anymore. The bubble size, which is periodic, remains as long type and no total suppression of the bubble is reached. As suggested by Hodson and Zhang [9] on this ultra-high-lift blade incoming wakes may not be enough to suppress the bubble.

Figure 17 shows the computed and measured isentropic Mach number distributions for steady and time averaged-unsteady distributions. The periodic impact of the wakes at the blade leading edge causes a shift of the angle of attack. This shift is quite well captured by the computations even if small discrepancies are visible. On the other hand the peak of velocity is clearly not well captured. De Saint Victor [38] reported that 1.5° deviation in the angle of attack largely affects the peak of velocity which may explain this discrepancy. Downstream the peak of velocity, even if the previously mentioned shift remains, the experimental tendency is quite well captured by the computation. The unsteady time-averaged experimental curve suggests the presence of a bubble between x/Cax=0.65 and x/Cax=0.90 which is also the case for the curve obtained by computation (see also in Fig. 16). The beneficial effect of the incoming wakes on the bubble is well visible on the isentropic Mach number distributions when comparing steady and unsteady results: massive separation of the boundary layer is prevented.

Copyright © 2011 by ASME

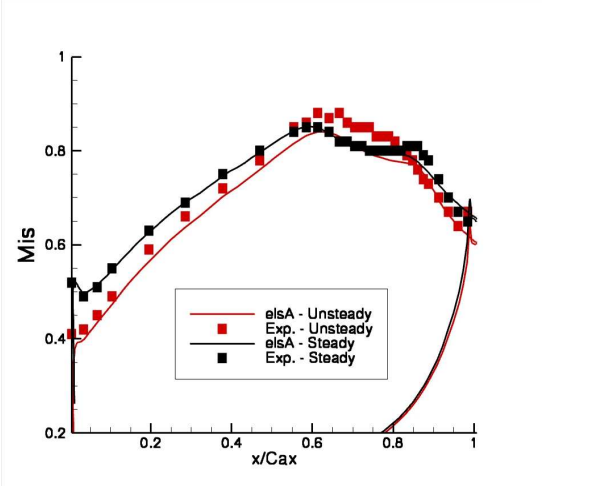

Figure 17: Comparison of computed and measured isentropic Mach numbers for the T106C cascade at Re_{2is}=100 000

CONCLUSION

The Menter and Langtry transition model completed by ONERA in-house correlations has been implemented in the RANS code *elsA* and tested on two experimental configurations: the T106C and T108 high lift blades. Steady results for the T106C blade indicates that the model completed by the ONERA in-house correlation can predict the blade performance very well for different Reynolds numbers and different turbulent intensity levels. However discrepancies have been noticed for the T108 blade. An analysis of the origin of these discrepancies is presented and suggestions for improving the transition model have been formulated. In the second part of this paper unsteady results for the T106C blade are presented. Unsteady computations have been performed in order to simulate the effect of the incoming wakes. An important modification, explained in this paper, has been applied to the transition model for permitting a proper modeling. The results are in quite good agreement with the experimental data. Further unsteady investigations are necessary to continue the model validation and improvement.

ACKNOWLEDGMENTS

The experimental results reported in this paper were provided by the Von Karman Institute in the framework of the European research programs TATMo (www.tatamo.eu) and UTAT (Unsteady Transition in Axial Turbines) for which ONERA was also involved. The authors would like to thank the Von Karman Institute partners who provided the experimental results and Edouard De Jaeghere, SNECMA, who provided the computational grids.

REFERENCES

[1] Gier, J., Franke, M., Hübner, N., and Schröder, T., 2010, "Designing Low Pressure Turbines for Optimized Airfoil Lift", ASME J. of Turbomachinery, **132**, 031008 pp. 1-11

[2] Hodson, H., and Howell, R.J., 2005, "The Role of Transition in High-Lift Low-Pressure Turbines for Aeroengines", Progress in Aerospace Sciences, **41**, pp. 419-454

[3] Horton, H.P., 1968, "Laminar Separation Bubbles in Two and Three Dimensional Incompressible Flow", Ph.D. thesis, Department of Aeronautical Engineering, Queen Mary College, University of London

[4] Hatman, A., and Wang, T., 1998, "Separated Flow Transition. Part 1-Experimental Methodology and Mode Classification", ASME Paper 98-GT-461

[5] Hatman, A., and Wang, T., 1998, "Separated Flow Transition. Part 2-Experimental Results", ASME Paper 98-GT-462

[6] Hatman, A., and Wang, T., 1998, "Separated Flow Transition. Part 3-Primary Modes and Vortex Dynamics", ASME Paper 98-GT-463

[7] Mayle, R.E., 1991, "The Role of Laminar-Turbulent Transition in Gas Turbines Engines", ASME J. of Turbomachinery, **113**, pp. 509-537

[8] Schulte, V., and Hodson, H.P., 1998, "Unsteady Wake-Induced Boundary Layer Transition in High Lift LP Turbines", ASME J. of Turbomachinery, **120**; pp. 28-35

[9] Zhang, X.F., and Hodson, H.P., 2005, "Combined Effects of Surface Trips and Unsteady Wakes on the Boundary Layer Development of an Ultra-High-Lift LP Turbine Blade", ASME J. of Turbomachinery, **127**, pp. 479-488

[10] Stieger, R., 2002, "The Effects of Wakes on Separating Boundary Layer in Low Pressure Turbines", Ph.D. thesis, University of Cambridge, UK.

[11] Coton, T., Arts, T., Lefebvre, M., and Liamis, N., 2003, "Unsteady and Calming Effects Investigation on a Very High-Lift LP Turbine Blade – Part 1: Experimental Analysis", ASME J. of Turbomachinery, **125**(2), pp. 281-291

[12] Raverdy, B., Mary, I., Sagaut, P. and Liamis, L., 2003, "High Resolution Large-Eddy Simulation of the Flow around a Low Pressure Turbine Blade", AIAA Journal, **38**(8), pp. 390-397

[13] Xiaohua, W., and Durbin, P.A., 2001, "Evidence of Longitudinal Vortices Evolved from Distorted Wakes in a Turbine Passage", J. Fluid Mechanics, **446**, pp. 199-228

[14] Sarkar, S., 2009, "Influence of Wake Structure on Unsteady Flow in a Low Pressure Turbine Blade Passage", ASME J. of Turbomachinery, **131**, 041016 pp. 1-14

[15] Menter, F.R., Langtry, R.B., Likki, S.R., Suzen, Y.B., Huang, P.G., and Völker, S., 2006, "A Correlation-Based Transition Model Using Local Variables – Part 1: Model Formulation", ASME J. of Turbomachinery, 128(3), pp. 413-423

Copyright © 2011 by ASME

[16] Langtry, R.B., 2006, "A Correlation-Based Transition Model Using Local Variables for Unstructured Parallelized CFD Codes", Ph.D. thesis, University of Stuttgart, Germany
[17] Suluksana, K., Dechaumphai, P., and Juntasaro, E., 2009, "Correlation for Modelling Transitional Boundary Layers under Influences of Freestream Turbulence and Pressure Gradient", International Journal of Heat and Fluid Flow, **30**, pp. 66-75
[18] Piotrowski, W., Elsner, W., and Drobniak, S., 2010, "Transition Prediction on Turbine Blade Profile with Intermittency Transport Equation", ASME J. of Turbomachinery, **132**, pp. 11-20
[19] Krause M., Behr, M., and Ballamann, J., 2008, "Modelling of Transition Effects in Hypersonic Intake Flows Using a Correlation-Based Intermittency Model", Proc. of the 15th AIAA International Space Planes and Hypersonic Systems and Technologies Conference, AIAA-2008-2598
[20] Sorensen, N., 2009, "CFD Modelling of Laminar-Turbulent Transition for Airfoils and Rotors using the γ - $\tilde{Re}_{\theta t}$ Model", Wind Energy, **12**(8), pp. 715-733
[21] Cheng, G., Nichols, R., Neroorkar, K.D., and Radhamony P.G., 2009, "Validation and Assessment of Turbulence Transition Models", Proc. of the 47th AIAA Aerospace Sciences Meeting, AIAA-2009-1141
[22] Obayashi, S., Misaka, T., and Toyoda, A., 2007, "An Application of Local Correlation-Based Transition Model to JAXA High-Lift Configuration Model", Proc. of the 25th AIAA Applied Aerodynamics Conference, AIAA-2007-4286
[23] Smirnov, E., and Smirnovsky, A., 2009, "Turbine Vane Cascade Heat Transfer Predictions Using a Modified Version of the γ - $\tilde{Re}_{\theta t}$ Laminar Turbulent Transition Model", Proc. of the 2009 International Symposium On Heat Transfer in Gas Turbine Systems
[24] Corral, R., and Gisbert, F., 2010, "Prediction of Separation-Induced Transition Using a Correlation-Based Transition Model", ASME Paper GT2010-23239
[25] Kelterer, M.E., Pecnik, R., and Sanz, W., 2010, "Computation of Laminar-Turbulent Transition in Turbomachinery Using a Correlation-Based γ - $\tilde{Re}_{\theta t}$ Transition Model", ASME Paper GT2010-22207
[26] Zhang, X.D., and GAO, Z.H., 2010, "Numerical Discussion on complete empirical correlation in Langtry's Transition Model", Applied Mathematics and Mechanics, 31(5), pp. 575-584
[27] Content, C., and Houdeville, R., 2010, "Application of the γ - $\tilde{Re}_{\theta t}$ Laminar Turbulent Model in Navier – Stokes Computations", Proc. of the 40th AIAA Fluid Dynamics Conference and Exhibit, AIAA-2010-4445, Chicago, Illinois, USA
[28] Menter, F.R., and Langtry R.B., 2009, "A Correlation-Based Transition Model Using Local Variables for Unstructured Parallelized Computational Fluid Dynamics Codes", AIAA Journal, 47(12), pp. 2894-2906
[29] Cambier, L. and Veuillot, J.P., 2008, "Status of the *elsA* CFD Software for Flow Simulation and Multidisciplinary Applications", Proc. of the 46th AIAA Aerospace Sciences Meeting and Exhibit, Reno, Nevada, USA.
[30] Arts, T., Michalek, J., and Monaldi, M., 2010, "Aerodynamic Performance of a Very High Lift Low Pressure Turbine Airfoil (T106C) at Low Reynolds and High Mach Number with Effect of Free Stream Turbulence Intensity, ASME Paper GT2010-22884
[31] Arts, T., Michálek, Y., Ilikan, A., 2009, VKI, "TATMo Task2B.4 – VKI", www.tatmo.eu
[32] Van Driest, E.R., and Blumer, C.R., 1963, "Boundary Layer Transition: Freestream Turbulence and Pressure Gradient Effects", AIAA Journal, **1**(6), pp. 1303-1306
[33] Abu Ghannam, B.J., and Shaw, R., 1980, "Natural Transition of Boundary Layers – The Effects of Turbulence, Pressure Gradient and Flow History", Journal of Mechanical Engineering Science, **22**(5), pp. 213-228
[34] Menter, F.R., 1994, "Two-Equation Eddy Viscosity Turbulence Models for Engineering Applications", AIAA Journal, **32**(8), pp. 1598-1605, AIAA Journal, **40**(2), pp. 254-266
[35] Marciniak, V., Kügeler, E., and Franke, M., 2010, "Predicting Transition on Low-Pressure Turbine Profiles", Proc. Of the 5th European Conference on Computational Fluid Dynamics ECCOMAS CFD, Lisbon, Portugal
[36] Fiala, A., 2009, "Report on CFD on separation bubble in turbine applications," MTU, TATMO report D3A.1.2.2, www.tatmo.eu
[37] http://gltrs.grc.nasa.gov/reports/2010/CP-2010-216112/09%20Session%2010/02%20Williams.pdf
[38] De Saint Victor, X., 2010, "Sensitivity of Numerical Simulations of Low-Reynolds Flow over the T106 Turbine Blade", ASME Paper GT2010-22903
[39] Spalart, P.R, and Rumsey, C.L., 2007, "Effective Inflow Conditions for Turbulence Models in Aerodynamics Calculations", AIAA Journal, **45**(10), pp. 2544-2553
[40] Lardeau, S., Leschziner, M.A., 2005, "Unsteady RANS Modeling of Wake-Blade Interaction: Computational Requirements and Limitations", Computers and Fluids, **34**, pp. 3-21
[41] Stieger, R.D., and Hodson, H.P., 2005, "The Unsteady Development of a Turbulent Wake through a Downstream Low-Pressure turbine blade Passage", ASME J. of Turbomachinery, **127**, pp. 388-394

Copyright © 2011 by ASME